Progress In Electromagnetics Research M, Vol. 74, 179–189, 2018

Printed Circularly Polarised Asymmetric Ultra-Wideband Antenna

Karavilavadakkethil C. Prakash, Puthiyapurayil V. Vinesh, Manoj Mani, Sumitha Mathew, Pezholil Mohanan, and Kesavath Vasudevan*

Abstract—Printed, circularly polarised, microstrip line fed antenna having asymmetric slotted structure is presented. Two antennas, antenna 1 (A1) and antenna 2 (A2), having the same design but radiating with opposite senses of circular polarisation are fabricated. The geometrical structure consists of uneven combination of elements fixed through parametric variations. The measurements yielded significant impedance bandwidth (IBW) and axial ratio bandwidth (ARBW) for axial ratio (AR) $\leq$ 3 dB. A1 offered IBW of 9.67 GHz (2.46–12.13 GHz, 132.6%), ARBW of 7 GHz (4–11 GHz, 93.33%) and a peak realised gain of 4.05 dBi. A2 offered IBW of 10.05 GHz (2.55–12.6 GHz, 132.7%), ARBW of 7.3 GHz (3.9–11.2 GHz, 96.7%) and a peak realised gain of 4.1 dBi. This constitutes a wide coverage of over 88% of the ultra-wideband (UWB) spectrum (3.1–10.6 GHz). Omnidirectional radiation patterns and marginal group delays are the other features of these antennas. The proposed design is validated through simulations and experimental investigations.

1. INTRODUCTION

Circularly polarized (CP) antennas are widely used in modern wireless communication systems. The tremendous needs for large system capacity and higher data rate in wireless systems have paved the path for the development of broadband CP antennas. The CP antenna is found to be highly effective in minimizing multi-path interferences or fading. Another advantage is that CP antenna is able to reduce the 'Faraday rotation' effect of the ionosphere. Considerable loss in signal strength occurs for linearly polarized signals compared to CP signals, which makes it a candidate for space telemetry applications of satellites, space probes and ballistic missiles to transmit or receive signals that have undergone Faraday rotation by travelling through the ionosphere. Moreover, it is not needed to strictly observe the orientation between transmitting and receiving antennas as there are no polarization mismatch losses. This feature is attractive for mobile satellite communications, where maintaining constant antenna orientation is not practical. The strength of the received signals is also fairly constant irrespective of the antenna orientation. These advantages make CP antennas very attractive for wireless systems [1]. Nowadays, researchers highly concentrate on designing wideband CP antennas with varied features to fulfill the requirements of wireless communication systems. Growing interest is observed in accommodating several operating frequencies in a single antenna which provide high IBW and ARBW. UWB electromagnetic pulses of nanosecond duration are very useful in communication field and widely explored for military and biotechnological applications. Therefore, broadband circularly polarized antennas have begun to replace narrowband circularly polarized elements such as microstrip patches [2].

Though there are different CP antenna geometries, they can roughly be divided into three types according to the mode of CP generation. The first type is patch antennas, which use the two orthogonal

Received 2 September 2018, Accepted 2 October 2018, Scheduled 16 October 2018

* Corresponding author: Kesavath Vasudevan (vasudevankdr@gmail.com).

The authors are with the Centre for Research in Electromagnetics and Antennas, Department of Electronics, Cochin University of Science and Technology, Kochi, Kerala 682022, India.

modes of TM_{01} and TM_{10} to obtain CP radiation. The second type is slot antennas, where instead of introducing a single polygonal slot or multiple slots on a patch antenna, a modified slot shape can be used to improve the CP bandwidth of patch antennas [1]. Due to the bidirectional radiation characteristics and lower quality factors, slot antennas have larger bandwidth than microstrip antennas. In conventional CP structures, the dimensions of the perturbation techniques critically affect the AR. Fabrication tolerances of perturbation segments may be minimized when slot antennas are used. Accordingly, slot antennas with perturbations are good candidates for broadband CP antennas. Slot antennas are complementary structures to the microstrip antennas by Babinet's Principle. Hence for CP operations, the perturbation technologies applied to slot antennas are good enough to design broadband CP antennas than patch antennas [3, 4]. Wong et al. have presented a printed ring-slot antenna that introduces asymmetry in the slot structure. A meandered slot section is used to perturb the symmetry of the ring-slot antenna, splitting the fundamental resonant mode into two orthogonal degenerate resonant modes for CP radiation [4]. The third type is the widely used spiral antennas and helical antennas, which incorporate the principles of travelling wave current along curved paths [1].

Major design strategies of antennas that have been investigated include an antenna having coplanar wave guide (CPW) fed quasi trapezoidal shaped radiating patch with two semicircular notches and two rectangular notches applied to the diagonal corners of the border ground [5], CPW fed square slot antenna with L-shape and crooked T-shape grounded strips square slot antenna [6], CPW fed square slot antenna with two corners connected by a strip line [7], antenna with a rectangular slot and horizontal stub [8], frequency selective surface backed wideband CP dual slot antenna [9], wideband CP perturbed psi shaped antenna [10], square slot antenna with antipodal Y strip [11], V shaped slot antenna [12], wideband slot antenna based on bent feed [13], slot antenna loaded by a multiple-circular-sector patch [14] and a square slot antenna with dual-sense circularly polarized radiation [15]. The highest percentage ARBW coverage of the UWB spectrum obtained by the antennas under study is 64% [13].

Slot antennas with large radiating aperture yield wider bandwidth without increasing the size and thickness. The ground plane size and placement of the slot on the ground plane affect the antenna's behaviour, to a great extent [3]. The conventional design strategies adopted in most of the reported works in literature [5–15] rely on symmetric antenna design technique, where ARBW values obtained do not cover the UWB spectrum to a good extent, with structures of comparable dimensions. Even though 100% ARBW was obtained with spiral and travelling wave structures [2], dimensions of such structures are more than doubled, compared to the proposed antenna in this work. This work is an investigation to adopt asymmetric design strategy, towards obtaining a compact structure that provides maximum percentage CP band coverage of the UWB spectrum. The structure described in this work offers better features in terms of dimensions, impedance and axial ratio bandwidths and CP band coverage of UWB spectrum than the existing antennas.

2. ANTENNA GEOMETRY AND DESIGN

2.1. Antenna Configuration

The geometry of the proposed antenna, antenna 1 (A1), is depicted in Figure 1. Another antenna, antenna 2 (A2), is also proposed, which is the exact mirror image of A1 in both planes with identical characteristics, whose geometry is shown in Figure 2. Figure 3 shows the geometrical structure of the top patch plane and bottom ground plane of A1 (seen through top plane) with dimensions labelled. These labels with corresponding dimensions are given in Table 1.

2.2. Design Steps

The design process of the proposed antenna A1 is explained through the evolution, composed of five intermediate structures as shown in Figure 4. Antenna 1a, which is the initial structure, has a microstrip line fed radiator having width of 3.72 mm, on the top plane of the substrate. Two copper strips, one attached perpendicularly on the tip and the other attached vertically on the right side of this microstrip feed line, form the radiating element. The off-center feeding structure yields wide bandwidth [8]. Hence the feeding structure is not centered about the top plane of the substrate but shifted slightly towards

Figure 1. Structure of the prosed antenna 1 (A1).

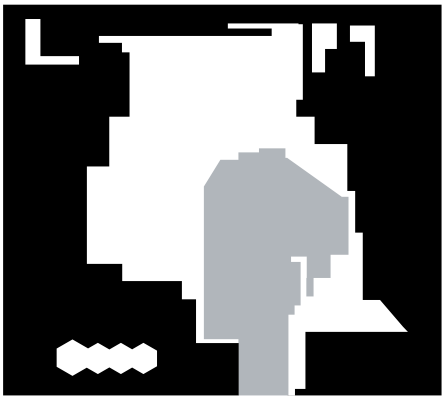

Figure 2. Structure of the proposed antenna 2 (A2).

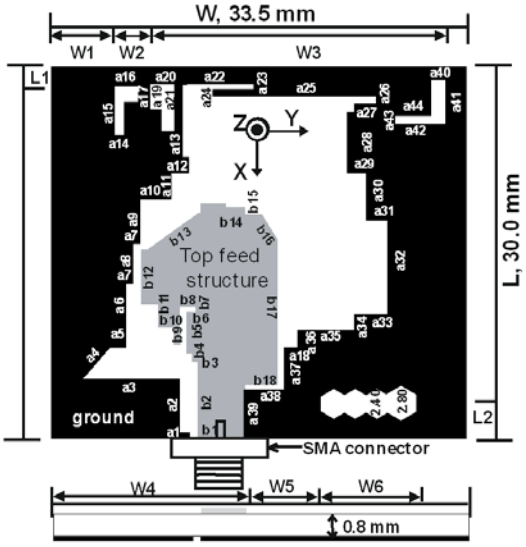

Figure 3. Geometrical structure of antenna 1 (A1) with dimensions labelled (top & side view).

the left. A rectangular strip (23.6×21.1 mm^2) is removed from the ground plane to form a wide slot. Simulation studies were carried out using ANSYS HFSS. Simulated reflection coefficient and axial ratio graphs of the antennas (antenna 1a to antenna 1e) are depicted in Figure 5 and Figure 6, respectively. These graphs are self narrative of the progress in IBW and ARBW. However, antenna 1a has the least impedance matching and is lacking in CP characteristics.

When a triangular portion is removed and two small copper strips are added to the upper portion of the feed line structure, antenna 1b is obtained. Now the matching has improved in the lower frequency region but still lacks in CP characteristics, as the axial ratio is well above the 3 dB limit. With a small triangular cut removed from the top and five copper strips of different dimensions attached to the left of the feed line, antenna 1c is evolved. Now the matching is better than that of its predecessor, but no improvement in the CP performance is observed, which is found to rather deteriorate. Antenna 1d is a modified version of antenna 1c, with the addition of four slots: one reverse 'L' slot on the top right corner of the border ground, two rectangular slots just beneath the feed line structure, and another inverted 'L' slot on the feed line structure as in Figure 4.

Now significant improvements are found in reflection coefficient and ARBW, in the upper frequency region. Design was further improved towards reaching the goal. Two sets, each of six strips having

Table 1. Dimensions of proposed antenna prototypes A1 and A2.

Label	Value (mm)	Label	Value (mm)	Label	Value (mm)	Label	Value (mm)	Label	Value (mm)
a1	00.80	a15	03.90	a29	1.55	a43	00.65	b13	05.16
a2	04.37	a16	01.90	a30	03.82	a44	02.95	b14	04.97
a3	07.83	a17	01.25	a31	01.71	b1	03.72	b15	00.57
a4	03.27	a18	01.00	a32	07.48	b2	06.20	b16	02.41
a5	01.32	a19	01.96	a33	02.70	b3	00.48	b17	11.71
a6	05.17	a20	01.90	a34	01.32	b4	00.45	b18	02.58
a7	00.58	a21	03.75	a35	04.56	b5	03.33	W1	05.10
a8	03.20	a22	05.73	a36	01.40	b6	00.72	W2	02.90
a9	03.60	a23	03.35	a37	03.36	b7	00.41	W3	23.80
a10	02.50	a24	00.57	a38	03.27	b8	01.20	W4	15.50
a11	02.10	a25	13.12	a39	04.02	b9	03.06	W5	06.24
a12	01.40	a26	00.53	a40	01.15	b10	01.30	W6	07.67
a13	05.80	a27	01.75	a41	03.50	b11	01.38	L1	01.60
a14	00.75	a28	05.63	a42	04.10	b12	04.45	L2	02.90

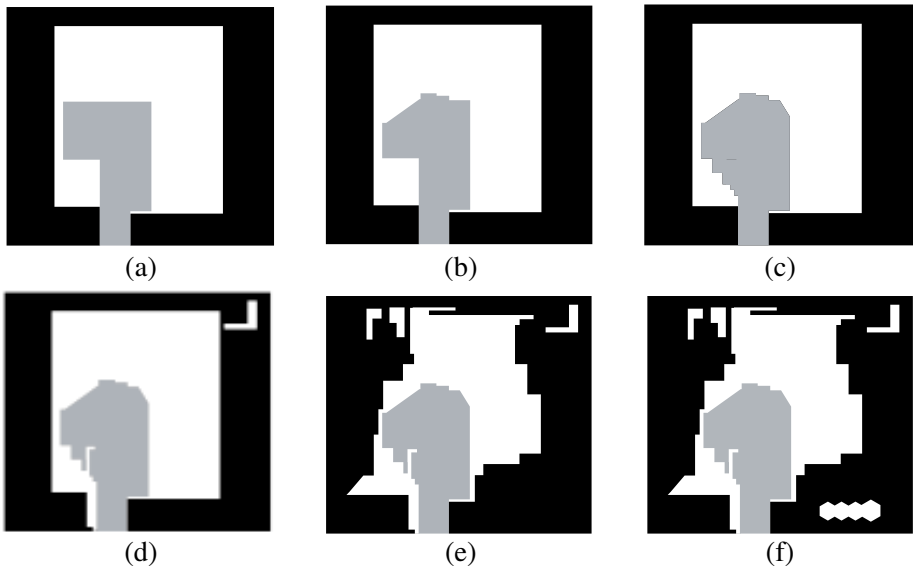

Figure 4. Evolution of proposed A1 (a) antenna 1a, (b) antenna 1b (c) antenna 1c, (d) antenna 1d, (e) antenna 1e and (f) proposed A1.

different dimensions, were added along the right and left portions of the ground. One strip was added along the top portion of the ground. Two inverted 'L' slots were added to the top left corner of the ground. IBW and ARBW were drastically improved. Finally, the proposed antenna structure, A1, was attained by introducing six hexagonal slots of different dimensions on the bottom right corner of the ground border. This provides full band coverage of UWB and a significant percentage coverage in ARBW. Thus the role of each element of the antenna at different frequencies in yielding good CP characteristics with good matching in the entire UWB spectrum was confirmed.

3. STUDY OF SURFACE CURRENT AND ELECTRIC FIELD PATTERNS

The contribution towards the ARBW by the hexagonal slots on A1 is better understood from the surface current pattern over A1 and its predecessor antenna 1e, which differ only in terms of these slots, at 11.2 GHz and $\omega t = 0°$ as shown in Figure 7. The distribution of surface current vector around these slots gives rise to horizontal and vertical components of electric field equal in magnitude and differ in phase by 90°. Similarly, each element of the structure contributes at different frequencies to enhance IBW and ARBW. Location of the feed was carefully optimized to obtain a good impedance match.

For a better understanding of the circularly polarized radiation mechanism, the simulated time-varying surface current distributions of the proposed antenna A1 at regular time phases from 0° to 270°, with an interval of 90° are depicted in Figure 8 at 6.85 GHz. It is observed that the surface current distributions at 0° and 180° are equal in magnitude and opposite in phase to that at 90° and 270°. On the feed structure of A1, at 0° phase, the surface current flows right, and at 90° phase the surface current flows downwards. Similarly, the surface current flows towards left at 180° phase and flows upwards at 270°. This shows that the surface current flows anticlockwise with respect to the viewer, and as such the proposed antenna A1 is right-hand circularly polarized (RHCP) in the $+Z$ direction. The electric field behaviour of A1 is also studied and shown in Figure 9. From the study of electric field vector in the ground plane of the antenna it is inferred that the proposed antenna A1 is left hand circularly polarized (LHCP) in the $-Z$ direction. The simulated time-varying surface current distributions of the proposed antenna A2 at regular time phases from 0° to 270°, with an interval of 90° are depicted in Figure 10, at 6.85 GHz. The electric field behaviour of A2 is also studied and shown in Figure 11. From the studies, it is understood that A2 radiates with LHCP in the $+Z$ direction and with RHCP in the $-Z$ direction.

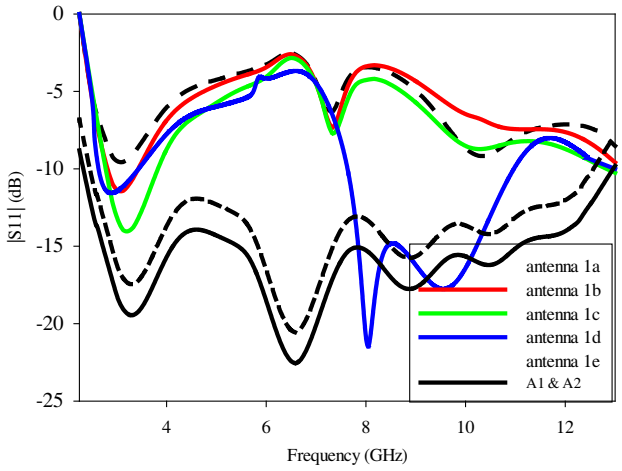

Figure 5. Simulated $|S_{11}|$ plots of antennas.

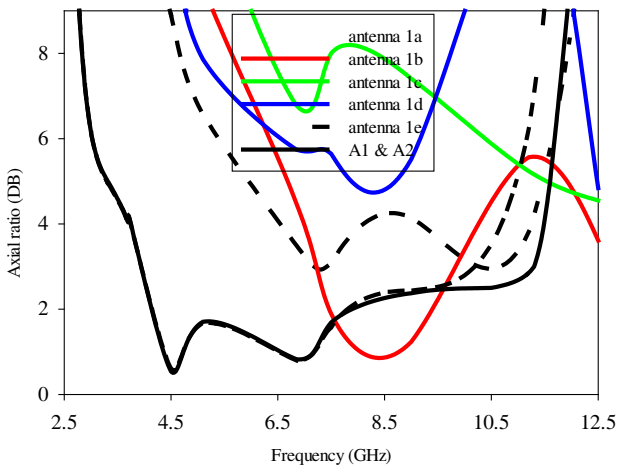

Figure 6. Simulated AR plots.

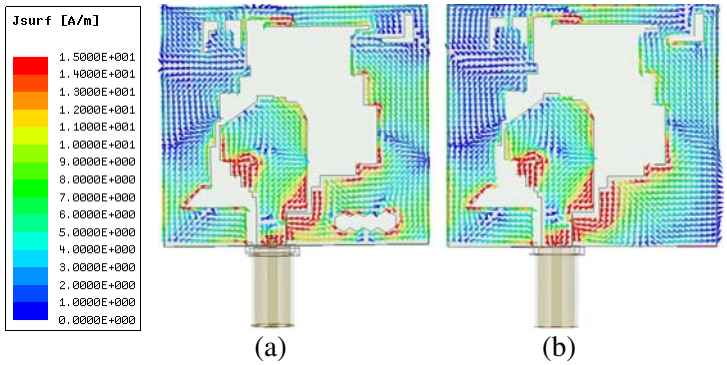

Figure 7. Surface current at $\omega t = 0°$, 11.2 GHz on (a) A1 and (b) antenna 1e.

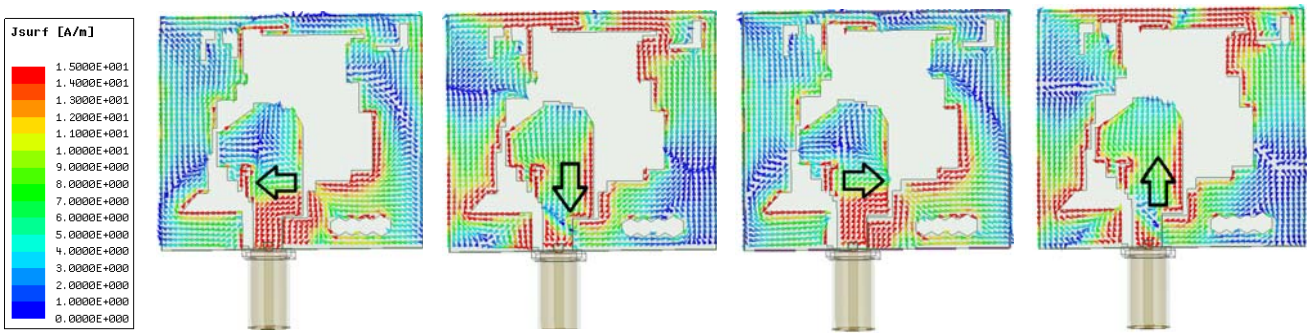

Figure 8. Surface current pattern on the proposed antenna A1.

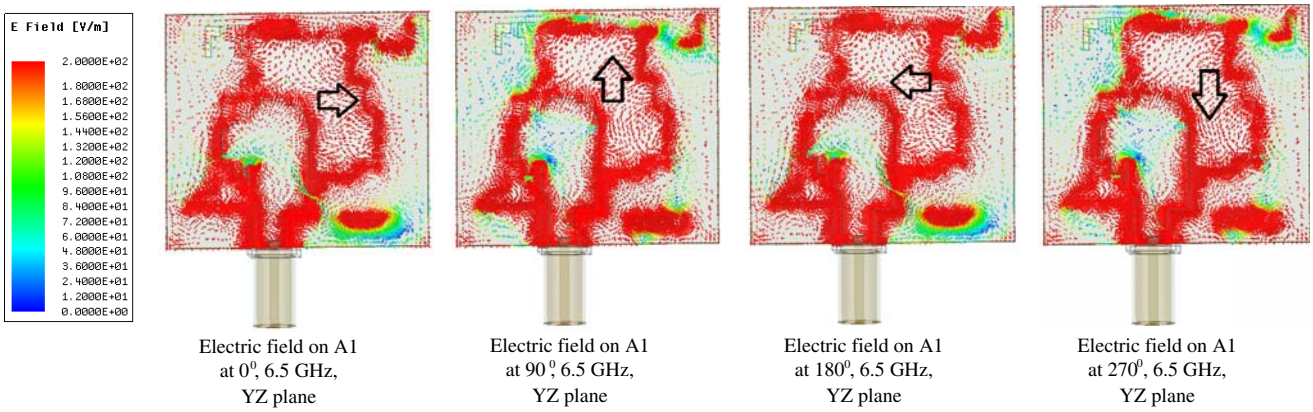

Figure 9. Electric field pattern on the proposed antenna A1.

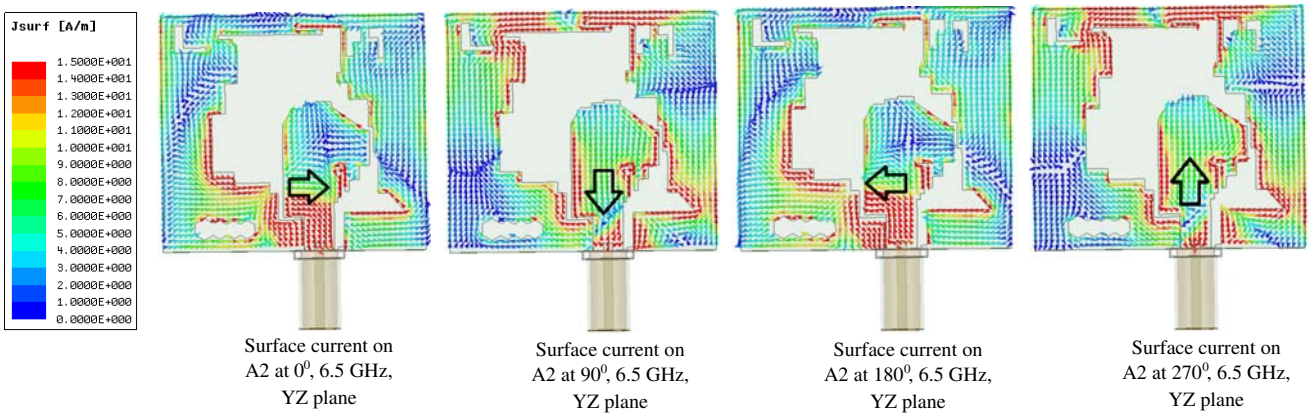

Figure 10. Surface current pattern on the proposed antenna A2.

4. MEASURED RESULTS AND DISCUSSION

4.1. Measurement of Reflection Coefficient and Axial Ratio

The proposed antenna structures were fabricated on FR4 substrate material with a dielectric constant 4.4, $\tan\delta = 0.02$ and size of $30 \times 33.5 \times 0.8\,\text{mm}^3$. The fabricated prototypes A1 and A2 were experimentally analysed using Agilent Vector Network Analyser PNAE 8362B, in an anechoic chamber.

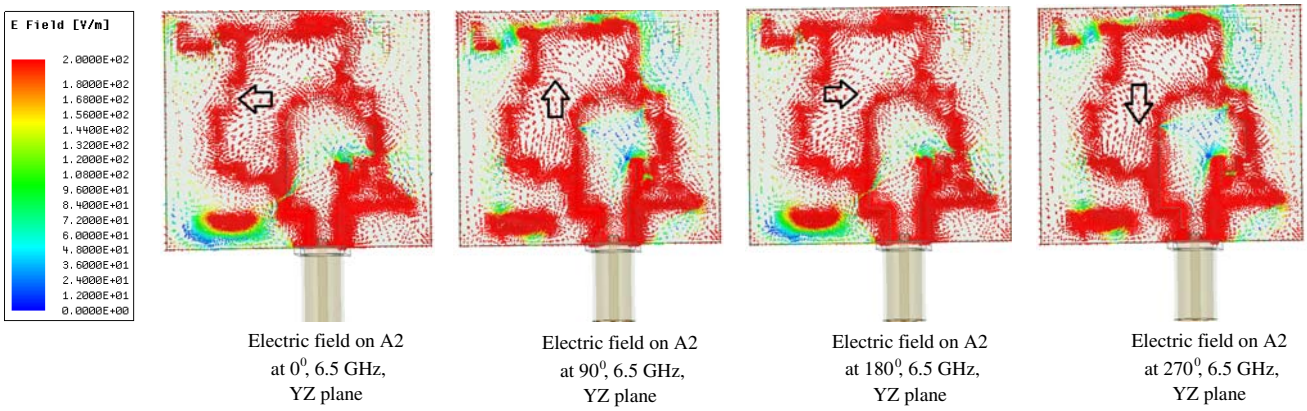

Figure 11. Electric field pattern on the proposed antenna A2.

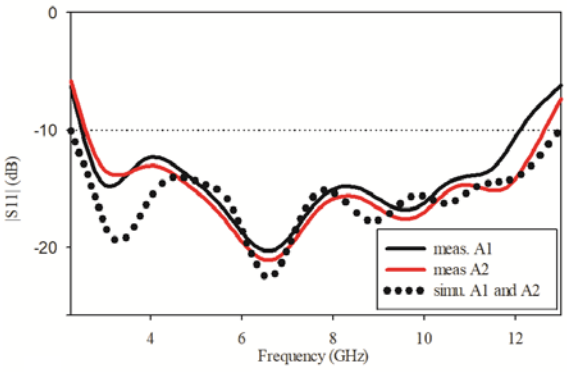

Figure 12. Measured and simulated $|S_{11}|$ plots of A1 & A2

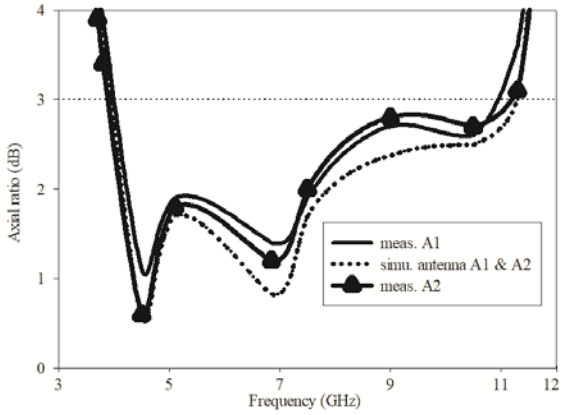

Figure 13. Measured and simulated axial ratio plots of A1 & A2.

Reflection coefficient measurements of A1 and A2 are plotted along with the simulation values in Figure 12. It can be seen from this figure that the simulated reflection coefficient plots coincide. Also, it is observed that there is close resemblance between measured and simulated results. Axial ratios of antennas A1 and A2 were measured using the standard setup in the anechoic chamber. These measurements along with simulated values are plotted as depicted in Figure 13. A1 offered IBW of 9.67 GHz (2.46–12.13 GHz, 132.6%) and ARBW of 7 GHz (4–11 GHz, 93.33%). A2 offered IBW of 10.05 GHz (2.55–12.6 GHz, 132.7%) and ARBW of 7.3 GHz (3.9–11.2 GHz, 96.7%).

The CP band coverage of UWB spectrum (3.1–10.6 GHz) by A1 is 88%, and that of A2 is 89.3%. These are the maximum achieved values compared with the antennas covered in the literature

4.2. Measurement of Realized Gain and Antenna Efficiency

Realised gain measurement using gain comparison method yielded average gain values of 3 dBi and 3.04 dBi for A1 & A2, respectively, in the operating frequency band. Peak gain values obtained were 4.0 dBi for A1 and 4.1 dBi for A2 at 8.72 GHz. Simulated and measured realized gain plots are depicted in Figure 14(a). The measured antenna efficiency plots are depicted in Figure 14(b). Peak values obtained were 92.71% at 3.3 GHz for A1 and 92.75% at 3.4 GHz for A2.

4.3. Measurement of Group Delay

Group delay measurements of A1 and A2 are shown in Figure 15. Measurements were carried out with two identical antennas each of A1 and A2, initially placed face to face and then side by side. The

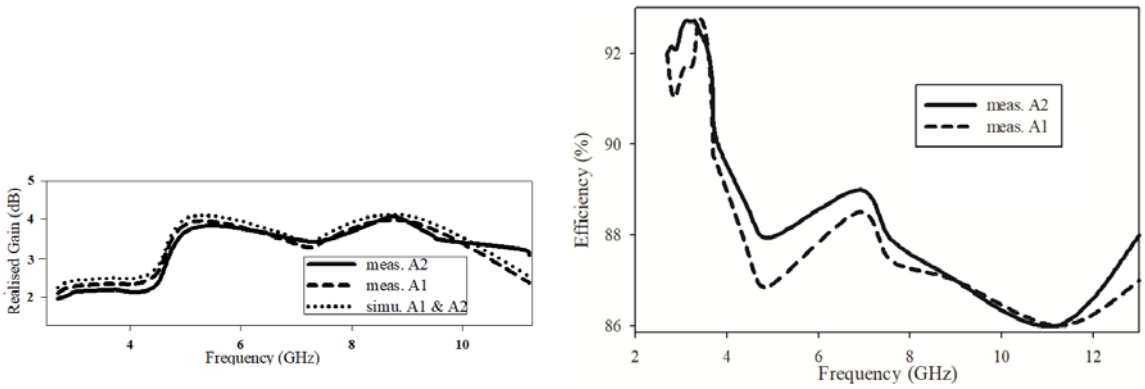

Figure 14. (a) Measured and simulated realized gain plots of the proposed A1 and A2. (b) Measured antenna efficiency plots of A1 and A2.

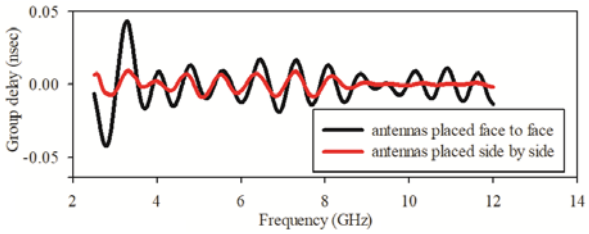

Figure 15. Measured group delay plots of the proposed A1 and A2.

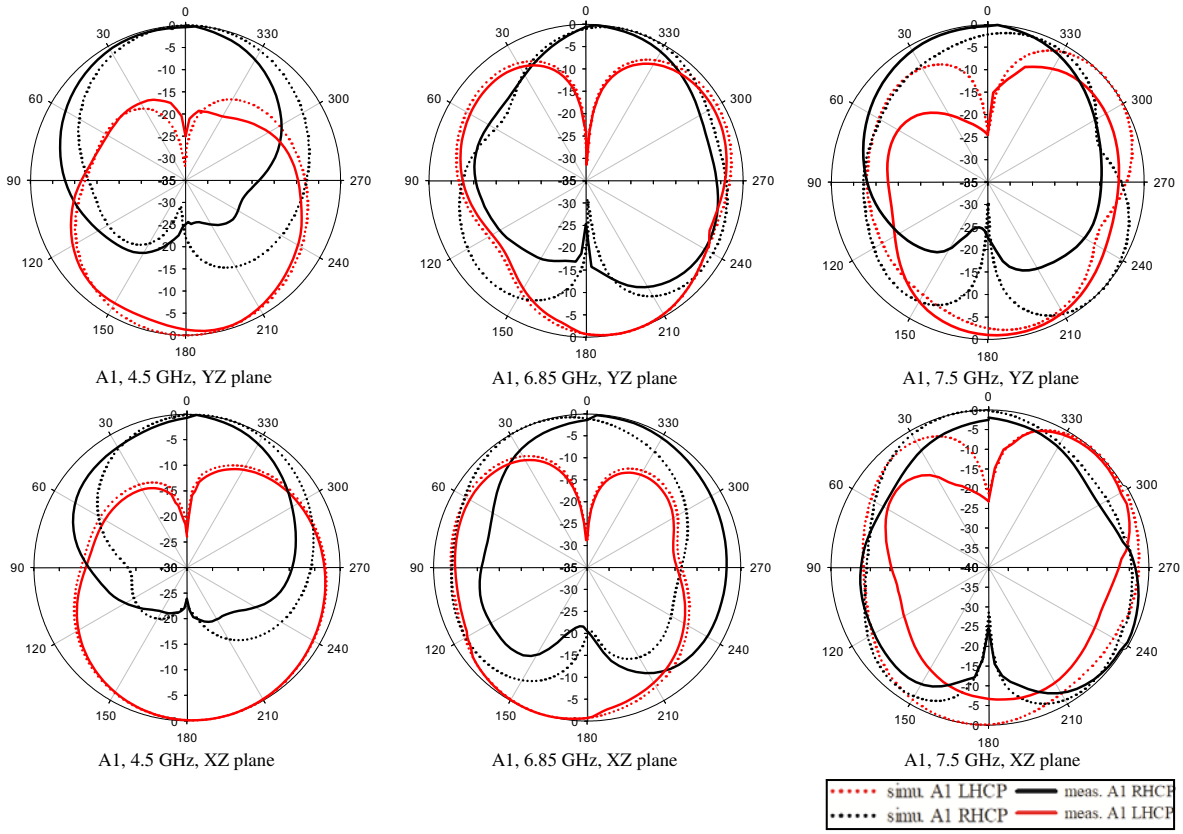

Figure 16. Normalised radiation patterns of A1 at three different frequencies.

measurement results of A1 and A2 coincide. It is observed that the group delay variations are less than 0.1 ns for both the antennas and are stable in the entire UWB spectrum. Consequently, it is inferred that the input signal suffers from negligible time delay in the operating range.

4.4. Measurement of Radiation Pattern

The simulated and measured far-field normalized radiation patterns of A1 and A2 in both XZ-plane and YZ-plane at frequencies 4.5 GHz, 6.85 GHz, and 7.5 GHz are plotted in Figure 16 and Figure 17. It is observed that the co-polarization is RHCP for A1 and LHCP for A2, whereas the cross-polarisation is LHCP for A1 and RHCP in the case of A2. The antenna has a wide half-power beam width at each measured frequency. The cross-polarisation level is lower than 20 dB. More than 20 dB isolation was observed between corresponding RHCP and LHCP patterns of both A1 and A2. Moreover, the radiation patterns of the antenna are stable and symmetrical in both XZ and YZ planes.

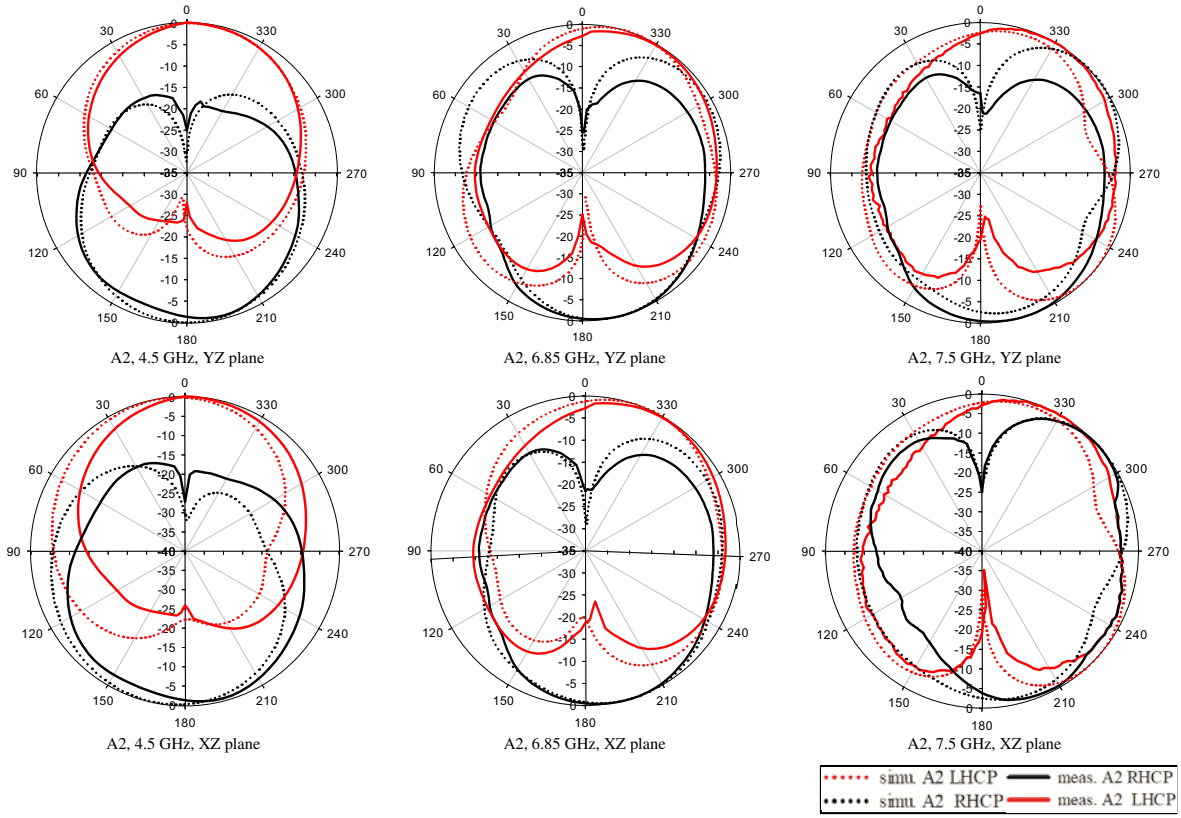

Figure 17. Normalised radiation patterns of A2 at three different frequencies.

(a) (b)

Figure 18. Photographs of fabricated antenna prototypes. Top and bottom views of (a) A1 (b) A2.

Table 2. Performance comparison of antenna prototypes A1 and A2.

Antennas under study	Size (mm^3)	IBW (GHz)	ARBW (GHz)	% CP of UWB
[4]	$100 \times 100 \times 1.6$	2.38–2.54	2.45–2.86	
[5]	$25 \times 25 \times 0.8$	2.76–14.82	4.2–6.13	25.7
[6]	$25 \times 25 \times 0.8$	3–11.1	5.05–7.1	27.33
[7]	$20 \times 20 \times 0.8$	2.95–14	3.73–7.1	44.9
[8]	$25 \times 25 \times 1.6$	3.5–9.25	4.6–6.9	30.7
[9]	$40 \times 40 \times 1.0$	3.72–9.2	4.5–8.0	46.7
[10]	$47.7 \times 58 \times 0.254$	5.0–7.0	5.0–6.0	13.3
[11]	$28 \times 28 \times 1.6$	3.25–8	4.4–6.67	30.27
[12]	$42 \times 44 \times 0.8$	2.19–4.6	2.2–4.9	24.0
[13]	$25 \times 25 \times 1.5$	3.2–8.5	3.3–8.1	64.00
[14]	$54 \times 54 \times 0.8$	1.68–3.97	1.89–3.95	11.33
This work, A1	$\mathbf{30 \times 33.5 \times 0.8}$	**2.46–12.13**	**4.0–11.0**	**88.0**
This work, A2	$\mathbf{30 \times 33.5 \times 0.8}$	**2.55–12.60**	**3.9–11.2**	**89.3**

These antennas offered omnidirectional patterns and are highly suitable for UWB communication. All measured results match very closely with the simulations. Performance comparison of the proposed antennas is done as shown in Table 2. The last column shows superior percentage in CP coverage of UWB spectrum by A1 and A2. Photographs of the fabricated antennas are depicted in Figure 18.

5. CONCLUSION

Printed asymmetric circularly polarised microstrip line fed antennas radiating with opposite senses of polarisation to each other, having wide IBW and ARBW, are proposed. The novelty is that with asymmetric structures these antenna prototypes exhibit nearly 90 percentage CP band coverage of the UWB spectrum. In terms of dimensions, this is an attractive feature compared to the existing antennas. In addition to that, these antennas exhibit moderate average gain, very good efficiency, omnidirectional radiation pattern and marginal group delay, suitable for UWB applications.

REFERENCES

1. Zhang, L., S. Gao, Q. Luo, P. R. Young, et al., "Single-feed ultra-wideband circularly polarized antenna with enhanced front-to-back ratio," *IEEE Trans. Antennas Propag.*, Vol. 64, 355–360, 2016.
2. Mao, S.-G., J.-C. Yeh, and S.-L. Chen, "Ultrawideband circularly colarized spiral antenna asing integrated balun with application to time-domain target detection," *IEEE Trans. Antennas Propag.*, Vol. 57, No. 7, 1914–1920, 2009.
3. Nakano, H. and J. Yamauchi, "Printed slot and wire antennas: a review," *Proceedings of the IEEE*, Vol. 100, No. 7, 2158–2168, 2012.
4. Wu, J., X. Ren, Z. Li, and Y. Yin, "Modified square slot antennas for broadband circular polarization," *Progress In Electromagnetics Research C*, Vol. 38, 1–14, 2013.
5. Shokri, M., V. Rafii, S. Karamzadeh, Z. Amiri, and B. Virdee, "Miniaturised ultra-wideband circularly polarised antenna with modified ground plane," *Electron. Lett.*, Vol. 50, 1786–1788, 2014.
6. Karamzadeh, S., V. Rafii, M. Kartal, and M. Dibayi, "Circularly polarized square slot antenna," *ACES Journal*, Vol. 30, No. 3, 327–331, 2015.

7. Karamzadeh, S., V. Rafii, M. Kartal, and H. Saygin, "Compact UWB CP square slot antenna with two corners connected by a strip line," *Electron. Lett.*, Vol. 52, 10–12, 2016.
8. Ellis, M. S., Z. Zhao, J. Wu, X. Ding, Z. Nie, and Q. H. Liu, "A novel simple and compact microstrip fed circularly polarized wide slot antenna with wide axial ratio bandwidth for C band applications," *IEEE Trans. Antennas Propag.*, Vol. 64, No. 4, 1552–1555, 2016.
9. Ding, K., C. Gao, T. Yu, and D. Qu, "Wideband CP slot antenna with backed FSS reflector," *IET Microw. Antennas Propag.*, Vol. 11, No. 7, 1045–1050, 2017.
10. Mondal, T., S. Maity, R. Ghatak, and S. R. B. Chaudhuri, "Design and analysis of a wideband circularly polarised perturbed psi-shaped antenna," *IET Microw. Antennas Propag.*, Vol. 12, No. 9, 1582–1586, 2018.
11. Nosrati, M. and N. Tavassolian, "Miniaturized circularly polarized square slot antenna with enhanced axial-ratio bandwidth using an antipodal Y-strip," *IEEE Antennas and Wireless Propagation Letters*, Vol. 16, 817–820, 2017.
12. Huang, H.-F. and B. Wang, "A simple V-shaped slot antenna with broadband circular polarization," *Progress In Electromagnetics Research Letters*, Vol. 67, 67–73, 2017.
13. Wu, Z., G. M. Wei, X. Li, and L. Yang, "A single-layer and compact circularly polarized wideband slot antenna based on bent feed," *Progress In Electromagnetics Research Letters*, Vol. 72, 39–44, 2018.
14. Trinh-Van, S., Y. Yang, K.-Y. Lee, and K. C. Hwang, "Broadband circularly polarized slot antenna loaded by a multiple-circular-sector," *Sensors*, Vol. 18, 1576–1588, 2018.
15. Xu, R., J.-Y. Li, J. Liu, S.-G. Zhou, K. Wei, and Z.-J. Xing, "A simple design of compact dual-wideband square slot antenna with dual-sense circularly polarized radiation for WLAN/Wi-Fi Communications," *IEEE Trans. Antennas Propag.*, Vol. 66, No. 9, 4884–4889, 2018.